ORIGINAL ARTICLE



Development of a minimized model structure and a feedback control framework for regulating photosynthetic activities

Lijiang Fu¹ · Govindjee Govindjee² · Jinglu Tan³ · Ya Guo^{1,3}

University of Missouri, Columbia, MO 65211, USA

Received: 12 August 2019 / Accepted: 4 November 2019 / Published online: 7 December 2019 © Springer Nature B.V. 2019

Abstract

Abbreviations

In this work, the main activities of the plant photosynthesis process are discussed to yield a minimized mathematical model structure with photosystem II (PSII) chlorophyll *a* fluorescence (ChlF) as a measurable output. After experimental validation of the model structure, we demonstrate that the states of the photosynthetic process may be observed by using this model and the extended Kalman filter method. We then show a feedback control framework that can be used to alter a given photosynthetic activity. The control framework is demonstrated with an example in which PSII ChlF is used as the feedback signal and light intensity is used as a controllable process input to regulate plastoquinone reduction. Although there are caveats, and further research is needed, the results lay the groundwork for further research on novel methods for optimization and regulation of photosynthetic activities, with a goal for sustainability.

LEF

Linear electron flow

Keywords Chlorophyll fluorescence · Photosynthesis · Modeling · Photosynthetic activity control

/ 100 C	iutions	LLI	Efficial electron now
A	Antenna molecules	NADPH	Nicotinamide adenine dinucleotide phosphate,
CEF	Cyclic electron flow		reduced form
ChlF	Chlorophyll a fluorescence	NPQ	Non-photochemical quenching of excited state
Cytb ₆ f	Cytochrome b ₆ f		of Chl
$C_{\rm a}$	Atmospheric CO ₂ concentration	OEC	Oxygen evolving complex
C_{i}	Internal CO ₂ concentration in the cells	P680	Reaction center Chl of Photosystem II, with
DPGA	Diphosphoglyceraldehyde		one of the absorption maxima at 680 nm
EKF	Extended Kalman filter method	PC	Plastocyanin
Fd	Ferredoxin	PGA	3-Phosphoglycerate
FNR	Ferredoxin-NADP reductase	PGAld	Phosphoglyceraldehyde
FQR	Ferredoxin-PQ reductase	Pheo	Pheophytin—primary electron acceptor in
H_{lumen}^+	H ⁺ (s) in the thylakoid lumen		Photosystem II
H ⁺ _{stroma}	H ⁺ (s) in the chloroplast stroma	PID	Proportion, integral, and derivative control
KABP	3-Ketoarabinitol-1,5-bisphosphate		method
		pmf	Proton motive force
Govindjee Govindjee gov@illinois.edu		PQ	Plastoquinone
		PQH_2	Plastoquinol
		PSI	Photosystem I
Ya Guo guoy@jiangnan.edu.cn; guoy@missouri.edu		PSII	Photosystem II
guoy	guoy e jiangnan.cuu.cn, guoy e missouri.cuu		Primary PSII plastoquinone (electron) acceptor
Key Laboratory of Advanced Process Control for Light Industry (Ministry of Education), Jiangnan University,		$egin{array}{c} Q_{ m A} \ Q_{ m B} \end{array}$	Secondary PSII plastoquinone (electron)
			acceptor
	i 214122, China	RuBP	Ribulose 1,5-bisphosphate
Department of Biochemistry, Department of Plant Biology, and Center of Biophysics & Quantitative Biology, University of Illinois at Urbana-Champaign, Urbana, IL 61801, USA		WWC	Water–water cycle
		XuBP	Xylulose-1,5-bisphosphate
01 111	more at Cream Champangn, Creama, ID 61661, Cort		

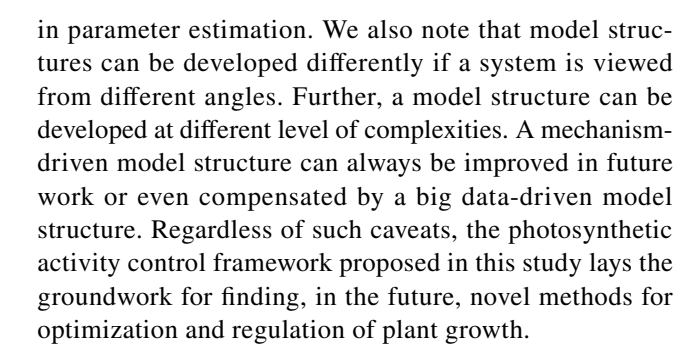


Introduction

Plants, algae, and cyanobacteria use solar energy to provide vital energy and food, through photosynthesis, to all living organisms (Shevela et al. 2019). Controlling photosynthetic activities is of interest in plant science as well as in automatic control technology. It is one of the major worldwide challenges to us all (Kennedy and Norman 2005). Greenhouse control strategies, based on plant photosynthesis, can reduce the waste of resources and maximize crop yield. It is thus important to develop a plant growth control strategy based on detailed knowledge of plant photosynthesis. To do so, a model to describe the major photosynthetic reactions is needed for control strategy development (Gopal 1996).

Specific aspects of photosynthesis of plants have already been modeled and simulated in different ways and at different levels of complexity (Lazár and Pospíšil 1999; Zhu et al. 2005, 2013; Laisk et al. 2006; Ebenhöh et al. 2011; Stirbet and Govindjee 2016; Feng et al. 2018; Xia et al. 2018). These models have either included only parts of the photosynthesis process or have described it in excessive details. Although they have provided important and significant understanding of the mechanism of photosynthesis, most have included too many variables and nonlinearities for control system design to optimize the efficiency of photosynthesis and carbohydrate production. In addition, a cross-scale modeling method of plant photosynthesis was established by Wu et al. (2019), which is a good way to show the impact of confounding factors on photosynthesis yield. This kind of model is important for simulating photosynthetic activities and crop growth with multiple environmental factors by using empirical information. However, it is limited only to simulation and hard to use for plant photosynthetic activities and growth feedback control due to lack of sensing physiology on-time and control strategy.

In this work, we developed a simplified model of photosynthesis that covers the process from light absorption to glucose production but, by design, ignores some details that have minor effects on the overall kinetic behavior of the process. Based on the developed model, *state estimation* (that is, estimation of the intermediate concentration based on the output) and control algorithms were designed for the regulation of photosynthetic activities by using chlorophyll *a* fluorescence (ChlF) as feedback signal. We know that the uniqueness of the estimates of model parameters will affect the applicability of the proposed model structure, but this can be improved in future work by calibration or optimization of model parameters within a certain range, based, e.g., on prior knowledge, or by experimentally measuring more variables as constraints



Model development

Photosynthesis includes both light-dependent and lightindependent (or dark) metabolic reactions. The dark reactions, leading to glucose formation, need the products of "light reactions," i.e., NADPH and ATP; since many enzymatic reactions of the "dark" phase are in fact light regulated via the ferredoxin: thioredoxin reductase (FTR) system, Buchanan (2016) prefers to refer to the "dark reactions," as "carbon reactions." These carbon reactions take place in the stroma matrix of the chloroplasts, while "the light reactions" take place in pigment protein complexes in the thylakoid membrane. As pointed out by one of us (Govindjee), in the footnote of the Buchanan paper, the true "light reactions" end after the primary charge separation steps; the rest of the reactions (the electron transfer and protonation steps) all can occur in the dark. The steps preceding the carbon reactions include absorption of photons, excitation energy transfer, primary photochemistry, and linear electron flow (LEF) from water to NADP⁺, leading to oxygen evolution, and NADPH & ATP production. For information on the different aspects of this process, see Mirkovic et al. (2016), Mamedov et al. (2017) and Govindjee et al. (2017). In addition, there is cyclic electron flow (CEF) around Photosystem I (see Joët et al. 2002). As noted above, there is ATP synthesis, which uses proton motive force (membrane potential as well as proton gradient) across the thylakoid membranes (Junge 2004), formed as a consequence of electron flow from water to NADP⁺. We also realize that there may even be other steps, some neglected, and some unknown. The "dark reactions" include the Calvin-Benson cycle, for the fixation of carbon dioxide, and production of carbohydrate. For a background on the various steps of photosynthesis, see Rabinowitch and Govindjee (1969), Blankenship (2002) and Shevela et al. (2013, 2019). Further, there exist regulatory mechanisms for the smooth operation of photosynthesis; these include, e.g., the non-photochemical quenching (NPQ) of the excited state of the chlorophyll a via the xanthophyll cycle, the "state transitions," as well as the activation of rubisco (Zhu et al. 2013; Demmig-Adams et al. 2014).



Photosynthesis has been modeled at different levels of complexity. If we were to use first-order reaction kinetics (Zhu et al. 2005) to describe the process, hundreds of equations would be involved, which, of course, would be theoretically more complete or accurate. However, a model involving too many reactions or state variables may not be very useful for engineering applications. It is difficult and time-consuming to estimate enormous number of model parameters from available experimental data. Moreover, it is quite difficult to build a control strategy based on a complex model structure. On the other hand, "second-order reaction kinetics" is an approximation for the real situation. Guo and Tan (2011, 2014) have shown that second-order reaction kinetics can successfully fit experimental data by simply redefining the model variables and the parameters used. Under this situation, the reaction rates are effective rates but still correspond to some known reactions, which can be much more easily explained than parameters in a neural network model structure. As a result, second-order reaction kinetics provide (s) a simpler approximation of the complex photosynthesis process. For a given system, different model structures may be developed if the system is viewed from different angles. To significantly reduce the number of state variables, we view the system reactions or the reactions in one reaction center as second-order reaction kinetics, even though it is not a precise description. We understand that some components may not be freely movable. The representation, used here, may skew the reaction rates from the first reaction kinetics and the reaction rates will have different units from the rates for the first reaction kinetics. We have also simplified some reactions, which will make the reaction rates as effective rates to represent the comprehensive effect of many reactions. Scientifically, this will not be accurate, but this will make control strategy development possible in engineering. Although the secondorder representation and reaction simplification make the reaction rates in this work not comparable with the rates for the first-order reaction kinetics in the available literature, they do not affect the concept of the framework that can be used to control photosynthetic activities and plant growth because other model structures in future work with more reasonable simplification can be embedded in the framework for plant growth control strategy development.

Light reactions and associated electron transport

The light reactions, including electron transport, consist of steps beginning with light absorption all the way up to the formation of NAPDH and oxygen. After absorption of photons by the antenna molecules, there are three pathways for the deactivation of excited chlorophyll molecules: excitation energy transfer leading to photochemical reaction (in the reaction centers), heat loss, and fluorescence emission. In this work, we have simplified

the description of antenna complexes, without distinguishing between the peripheral antenna and the core antenna. The total number of antenna molecules (labeled as A) per reaction center is taken as 300 (Zhu et al. 2005). The process of light absorption and antenna deactivation is expressed as follows:

$$A \xrightarrow{k_1 * u} A^* \tag{1}$$

$$A^* \xrightarrow{k_2} A + fluorescence$$
 (2)

$$A^* \xrightarrow{k_3} A + heat \tag{3}$$

where k_1 represents light-capture efficiency, u represents light intensity, and k_2 and k_3 represent the initial dissipation rate as fluorescence and heat, respectively.

Photon energy is lost, to some extent (\sim 5%), as heat or fluorescence, but most of it (\sim 95%) is used for primary photochemistry (charge separation at the reaction centers) that leads to electron transfer and photosynthesis (Rabinowitch and Govindjee 1969; Blankenship 2002). Following many others (e.g., Zhu et al. 2005), we describe the reactions in PSII reaction centers as follows (for details of PSII, see chapters in Wydrzynski and Satoh (2005)):

$$A^* + P680 \stackrel{k_4}{\rightleftharpoons} A + P680^*$$
 (4)

$$P680^* + Pheo \stackrel{k_6}{\rightleftharpoons} P680^+ + Pheo^-$$
 (5)

where P680, P680*, and P680⁺ represent the PSII reaction center, its excited state, and its oxidized form; Pheo and Pheo⁻ are the primary electron acceptor pheophytin of PSII, in the oxidized and the reduced state.

The reduction of P680⁺ occurs ultimately with electrons originating in water via several intermediates: Yz, a tyrosine, and the "S" states (related to Mn complexes). In the Kok–Joliot cycle (Kok et al. 1970; Mar and Govindjee 1972) for water oxidation, these steps also involve the release of protons in the lumen (see, e.g., Najafpour et al. 2013). For simplicity, we neglect the detailed process of water oxidation here. However, the oxidation of water and the reduction of P680⁺ (with electrons originating in water) is expressed as follows.

$$4P680^{+} + 2H_{2}O \xrightarrow{k_{8}} 4P680 + 4H_{lumen}^{+} + O_{2}$$
 (6)

On the electron acceptor side of PSII, Pheo⁻ (see Eq. 5) transfers its electron to Q_A , a plastoquinone, which is bound tightly on the D2 protein in PSII; this process is expressed as:

$$Pheo^{-} + Q_{A} \underset{k_{10}}{\overset{k_{9}}{\longleftrightarrow}} Pheo + Q_{A}^{-}$$
 (7)

where $Q_{\rm A}^-$ is the reduced form of $Q_{\rm A}$.



In turn, the electron on $Q_{\rm A}^-$ reduces $Q_{\rm B}$ (another plastoquinone molecule, bound to the D1 protein in PSII), which uses two electrons (one by one), all originating ultimately from the oxidation of water molecules. These processes are described (see, e.g., Velthuys and Amesz 1974; Guo and Tan 2011) as:

$$Q_{\mathbf{A}}^{-} + Q_{\mathbf{B}} \underset{k_{12}}{\overset{k_{11}}{\longleftrightarrow}} Q_{\mathbf{A}} + Q_{\mathbf{B}}^{-} \tag{8}$$

$$Q_{\rm A}^- + Q_{\rm B}^- \underset{k_{\rm 1A}}{\overset{k_{\rm 13}}{\Longleftrightarrow}} Q_{\rm A} + Q_{\rm B}^{2-} \tag{9}$$

After having received two electrons, $Q_{\rm B}^{2-}$ accepts two protons, one by one from the nearby amino acids, which ultimately obtain the protons from the stroma. A unique molecule of bicarbonate, bound on the non-heme iron, between $Q_{\rm A}$ and $Q_{\rm B}$, is involved in the delivery of the second proton (Shevela et al. 2012). Once $Q_{\rm B}H_2$, which is PQH₂, is formed, it diffuses into the membrane and is replaced by a plastoquinone (PQ) molecule from the membrane. Ultimately, the protons (in PQH₂) end up in the lumen. The exchange process of PQ is represented as:

$$Q_{\rm p}^{2-} + \rm PQ + 2H_{\rm errors}^{+} \xrightarrow{k_{15}} Q_{\rm B} + \rm PQH_2 \tag{10}$$

Cytochrome b₆f (Cytb₆f) is the PQ-plastocyanin oxidoreductase, which sits in-between PSII and PSI, and functions to transfer electrons from PQH₂ to plastocyanin (PC) (Cramer and Kallas 2015). Further, Cytb₆f acts to release additional four protons in the lumen, using the Q-cycle for each molecule of PQH₂ (Sacksteder et al. 2000; Ebenhöh et al. 2014). The following equation expresses the overall process at the Cytb₆f complex:

$$PQH_2 + 2PC + 2H_{\text{stroma}}^+ \stackrel{k_{16}}{\rightleftharpoons} PQ + 2PC^- + 4H_{\text{lumen}}^+$$
 (11)

With the help of PC-ferredoxin oxidoreductase (Photosystem I, PSI), electrons from the reduced PC (PC⁻) are transferred to ferredoxin (Fd) (Ebenhöh et al. 2014) and expressed as (for details of PSI, see Golbeck 2006):

$$PC^{-} + Fd \underset{k_{19}}{\overset{k_{18}}{\longleftrightarrow}} PC + Fd^{-}$$
 (12)

The last step in the linear electron flow (LEF) of the "light reactions" is the formation of NADPH, which is catalyzed by FNR (Ferredoxin-NADP reductase); here, the electrons are transferred to NADP⁺ from the reduced Fd (Ebenhöh et al. 2014; also see Stirbet and Govindjee 2016). Considering the steps of LEF leading to the formation of NADPH, which includes the oxidation of two molecules of water, we have the release of one molecule

of O_2 and the formation of two molecules of NADPH (see Allen 2002; Wydrzynski and Satoh 2005). For the NADPH formed, the equation can be written as:

$$2Fd^{-} + NADP^{+} + H_{\text{stroma}}^{+} \underset{k_{21}}{\overset{k_{20}}{\Longleftrightarrow}} 2Fd + NADPH$$
 (13)

With the protons pumped into the lumen, the proton motive force (pmf) is built up, and then the formation of ATP takes place in the stroma (Junge 2004). Further, it is generally assumed that 14 protons are required to form three ATP molecules by the ATP synthase, with 14 c-subunits (Allen 2002). Just as ATP, NADPH is also formed in the stroma (Kramer and Evans 2011). Both the ATP and NADPH, formed as a result of the "light reactions," are then used to run the carbon cycle, the Calvin–Benson cycle (Allen 2002). Following all that is known for a long time, we repeat that two molecules of water are oxidized to give one molecule of oxygen, and two molecules of NADP+ are reduced to NADPH.

For the fixation of one molecule of CO₂, the system needs two molecules of NADPH and three molecules of ATP (Laisk et al. 2006). As described above, oxidation of two molecules of water produces four protons in the lumen; further, eight protons are pumped into the lumen whenever the Q-cycle operates (Crofts 2004). We know that the linear electron transfer alone cannot meet the demand of the Calvin-Benson cycle. In other words, the oxidation of two molecules of water are not enough to provide all the protons needed for ATP synthesis; two extra protons are necessary besides what LEF can provide. Kramer and Evans (2011) discussed several different mechanisms that provide these extra protons, which do not generate NADPH: cyclic electron flow (CEF) around PSI, the water-water cycle (WWC), the malate valve, and the plastoquinol oxidase. For simplicity, we assume here that all extra protons come from the cyclic electron flow (CEF), since this has been thought to be the major ATP/NADPH balancing pathway (Kramer and Evans 2011). The most important CEF around PSI is assumed to involve ferredoxin-PQ reductase (FQR), which transfers electrons from reduced Fd (Fd⁻) to PQ (Ebenhöh et al. 2014; Finazzi and Johnson 2016; Allen 2003). Thus, we express the CEF as:

$$2Fd^{-} + PQ + 2H_{stroma}^{+} \xrightarrow{k_{22}} 2Fd + PQH_{2}$$
 (14)

It has been generally accepted that 14 protons in the lumen are used to make three molecules of ATP in the stroma, using the available proton motive force. We express this process as:

$$3ADP + 14H_{lumen}^{+} \xrightarrow{k_{23}} 3ATP + 14H_{stroma}^{+}$$
 (15)

When two molecules of water are oxidized and three molecules of ATP are formed, we have an 'exact' match with their



consumption in the Calvin-Benson cycle (Kramer and Evans 2011). It is generally acknowledged that it is a self-sufficient relationship between the ATP produced from the photoreaction phase and the ATP required for carbon fixation. That is to say that we assume that the NAPDH and ATP used for carbon reactions are all from the products of the "light reactions." However, recent studies show that possible additional mechanisms involved will play a role in the Calvin–Benson cycle. For instance, other anabolic processes consume a small amount of ATP or additional ATP uptake would be needed when photosynthesis does not produce sufficient ATP for CO₂ fixation and other anabolic reactions. The plastidic ATP/ADP transporter translocates relatively small amounts of ATP generated in the mitochondria from cytosol to stroma (Winkler and Neuhaus 1999). For simplification, some detailed reactions are not included in the model developd here.

For the integrity of the system, and the system's ability to resist damage caused by strong light, regulatory mechanisms are involved.

Regulatory high-energy quenching (qE) mechanism

When light is too strong, plants initiate a regulatory mechanism, using NPQ of the excited state of chlorophyll, which protects and stabilizes the system (see Papageorgiou and Govindjee 2014; Demmig-Adams et al. 2014), while the excess energy is dissipated as heat (Matuszynska et al. 2016). Further, Chl a fluorescence data have been shown to reflect photosynthetic characteristics of plants and the impact of external conditions on them (see, e.g., Guo and Tan 2015; Stirbet et al. 2018). For examples of measurements and analysis of NPQ in studies that have led to models, see Ebenhöh et al. (2011, 2014), Matuszynska et al. (2016), and Snellenburg et al. (2017). Although the theory of NPQ is described in great details in some of these studies, models used there are just too complex with too many model parameters that are inconvenient for practical engineering use. Further, we have noticed inaccuracies in parameter fitting with experimental data (unpublished data of the authors), and practical application for engineering purposes seem difficult. In view of the above, the disadvantage of these models is obvious. Thus, one of the goals of this work was to find a way to describe NPQ in as simple a term as possible.

The NPQ, as a photo-protection mechanism, has three quenching components: energy dependent (qE), state transition (from state I to state II; qT), and photoinhibition (qI) (Demmig-Adams et al. 2014; Ebenhöh et al. 2011). The major component is qE, which we will discuss in our proposed model structure (see below; Eqs. 16 and 17). We have left out qI since it involves damage of the system by high light, and qT, which is related to the adjustment of the relative absorption cross section of PSI and PSII, accounting, usually, for only a small part of total quenching (see, e.g. Ebenhöh et al.

2011). Thus, qI and qT are neglected in our analysis here. Under high light conditions, qE quenching is triggered by high proton concentration in the lumen, and it is known to be linked to the xanthophyll cycle, where zeaxanthin acts as a direct quencher (for a time line of discoveries, see Papageorgiou and Govindjee 2004). Zeaxanthin is formed from de-epoxidation of violaxanthin (expressed as N_o) under the H⁺ gradient in the lumen. Thus, the H⁺ concentration indirectly determines the NPQ efficiency, and when the [H⁺] on the lumen side of the thylakoid membrane is high, the NPQ efficiency is also high. The interconversion of zeaxanthin and violaxanthin in the xanthophyll cycle can be expressed simply as:

$$N_0 \stackrel{k_{24}[\mathrm{H}^+_{\mathrm{lumen}}]}{\longleftrightarrow} N \tag{16}$$

where N is the relative concentration of zeaxanthin, with $N+N_0$ being 1. Here, we assume that the transformation of violaxanthin to zeaxanthin, and the reverse, is linear in order to fit the experimental data and the actual application of the system. As is generally accepted, zeaxanthin increases the rate constant of heat dissipation (see, e.g., Zhu et al. 2013). Thus, we can modify Eq. (3) as follows:

$$A^* \xrightarrow{k_3\{1+[N]\}} A + heat \tag{17}$$

The carbon reactions (or dark reactions)

The Calvin–Benson cycle (the carbon cycle) is a part of dark reactions in photosynthesis, and its reaction site is stroma, the chloroplast matrix. This cycle has three major stages: carboxylation of RuBP by CO₂, reduction of CO₂, and regeneration of ribulose 1,5-bisphosphate (RuBP) (see, e.g., Bassham 2003). Most plants integrate (and thus fix) CO₂, by binding it to the second carbon of the 5-carbon RuBP, using RuBP carboxylase-oxygenase (rubisco). The COO group, thus formed, can be easily reduced. Further, the sixcarbon compound, thus formed, is extremely unstable and immediately gives two molecules of 3-phosphoglycerate, a three-carbon compound. The latter is then phosphorylated by ATP (formed by ATP synthase) to 1, 3 diphosphoglyceric acid (DPGA), which is then reduced by the NADPH generated through the two-light reaction, two-pigment system of electron transport (see above "Light reactions and associated electron transport" section) to triose phosphate. Later, after a series of biochemical reactions, one of the triose phosphate molecules-leaving the cycle- is used to synthesize glucose. In balance, six turns of the cycle produce one molecule of hexose. On the other hand, the cycle includes the regeneration of a ribulose-1,5-diphosphate molecule, which restarts the cycle. The above steps are described below in details, with equations.



Carboxylation of CO₂

This is a complex biochemical process that includes intermediates such as 3-ketoarabinitol-1,5-bisphosphate (KABP) and xylulose-1,5-bisphosphate (XuBP), as well as "Rubisco Activation" (Portis 2003). Here, a simplistic chemical reaction formula is used to approximate its representation. One molecule of RuBP combining with one molecule of CO₂ forms two molecules of 3-phosphoglycerate (PGA) under the catalytic action of Rubisco. This is shown as:

$$RuBP + CO_2 + H_2O \xrightarrow{k_{26}} 2PGA$$
 (18)

where CO_2 is for the concentration of intercellular CO_2 ; it is expressed as C_i , and k_{26} is the reaction rate constant related to carboxylation of RuBP.

Reduction of CO₂

PGA is reduced to phosphoglyceraldehyde (PGAld) using ATP and NAPDH generated during the light reactions and the associated electron transfer (see "Light reactions and associated electron transport"). After all these steps, the photosynthetic energy storage process is over, and this last process is described as:

$$PGA + ATP \xrightarrow{k_{27}} DPGA + ADP$$
 (19)

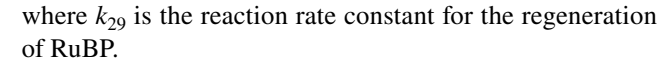
$$DPGA + NADPH + H^{+} \xrightarrow{k_{28}} PGAld + NADP^{+}$$
 (20)

where DPGA is for diphosphoglyceraldehyde, and k_{27} and k_{28} are the rate constants for the chemical reactions involved in phosphorylation and in the reduction of carbon.

Regeneration of RuBP

In the Calvin–Benson cycle, three molecules of CO₂ are fixed, and six molecules of PGAld are produced. Five PGAld molecules are used to synthesize three molecules of RuBP, which are then re-used to fix CO₂. To make one hexose molecule, we need the fixation of six molecules of CO₂ (Wang et al. 2018). Further, the fixation of one CO₂ molecule produces two molecules of PGAld; for this, two molecules of NADPH and three molecules of ATP, generated by the operation of two light reactions, are used. The regeneration of RuBP is essential for further CO₂ fixation and, thus, for plant growth. The overall reaction for this regeneration is represented as:

$$5PGAld + 3ATP \xrightarrow{k_{29}} 3RuBP + 3ADP$$
 (21)



Carbon dioxide enters plants through stomata on the leaves; this process is affected by environmental factors such as light intensity and atmospheric CO_2 concentration (C_a) (Farquhar et al. 1980). Earlier studies usually used steadystate representations; further, the earlier models were very complicated (Farguhar et al. 1980; Katul et al. 2000). Here in our work, we have greatly simplified the model. Some steps related to CO₂ absorption, including photorespiration, stomatal conductance, or other substance limitations, have been ignored in our model. For example, we can neglect CO₂ concentration in greenhouses, since it can be regulated there. Furthermore, photorespiration usually occurs under high light intensity and low CO₂ conditions (Farquhar et al. 1980). Nonetheless, CO₂ transport depends on the concentration difference of CO₂ between the inside and the outside of the cell membrane. Thus, we have used the Fick's law to directly express this process (Wang et al. 2018):

$$\frac{\mathrm{d}C_{\mathrm{i}}}{\mathrm{d}t} = k_{30}(C_{\mathrm{a}} - C_{\mathrm{i}}) \tag{22}$$

where k_{30} is for the diffusion coefficient of CO_2 , and C_a and C_i are for the ambient and the internal CO_2 in the cells. As C_a increases, the rate of diffusion of CO_2 into cells increases; however, side effects may occur when C_a is too high (Harley et al. 1992).

The final step in photosynthesis is the production of carbohydrate. We know that stable carbohydrates are usually stored in plants in the form of starch and sucrose, but they are formed from glucose ($C_6H_{12}O_6$), which is the direct product of photosynthesis. The concentration of glucose, formed through photosynthesis, can be considered to represent the biomass of the plant. Thus, we have included glucose in our model and the last step is represented as:

$$PGAld \xrightarrow{k_{31}} 1/2 \text{ glucose}$$
 (23)

where k_{31} is the reaction rate constant for the production of glucose.

Figure 1 shows a simple diagram of the whole processes of photosynthesis, from the absorption of light to the formation of glucose, where the purple solid arrows indicate the transfer of electrons among the intermediates shown, and the red dotted arrows indicate the dynamic process of H^+ transfer to the lumen of the thylakoid membrane. Note that some of photosynthetic steps and related enzymes are not shown in Fig. 1 or included in the model for simplification. This includes PSI system since PSI is much more resistant to environmental changes compared to PSII (Butler 1978; Guo and Tan 2011). Further, fluorescence from PSI contributes only a small amount of the total ChIF and mainly to F_0 , the minimal fluorescence (Lazár 2006). For the meaning of



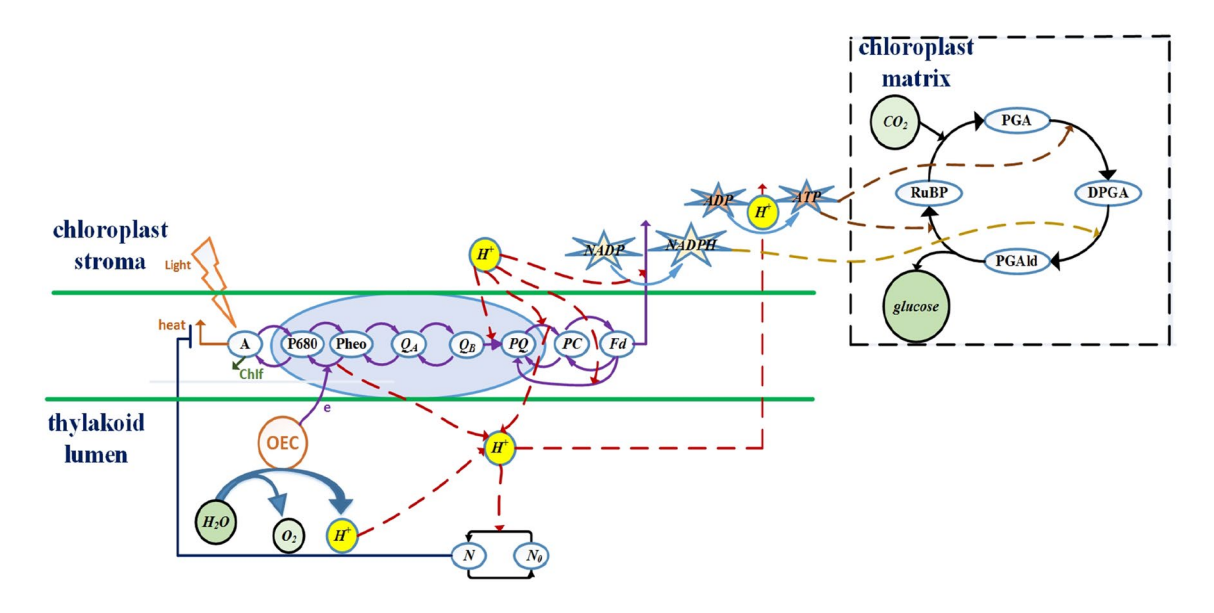


Fig. 1 A simple diagram of the whole processes of photosynthesis from light absorption to the formation of glucose. For full form of the symbols, see the list of abbreviations

Table 1 Sums of relative concentrations of intermediates

$A + A^* = 300$	$Q_{\rm B} + Q_{\rm B}^- + Q_{\rm B}^{2-} = 1$
$P680 + P680^* + P680^+ = 1$	$PQ + PQH_2 = PQ_0$
$Pheo + Pheo^- = 1$	$PC + PC^{-} = PC_0$
$Q_{\rm A} + Q_{\rm A}^- = 1$	$Fd + Fd^- = Fd_0$
$ATP + ADP = ATP_0$	$NADPH + NADP^{+} = NADPH_{0}$

the symbols and abbreviations used in the diagram, see the above text.

Concentrations of the components

The total concentration or probability of the presence of some of the intermediates, such as all the $Q_{\rm A}$ (i.e., both $Q_{\rm A}$ and $Q_{\rm A}^-$), all the $Q_{\rm B}$ (i.e., all its three forms: $Q_{\rm B}$, $Q_{\rm B}^-$, and $Q_{\rm B}^2$), total P680 (i.e., P680, P680* and P680*), and total Pheo (i.e., both Pheo and Pheo⁻), can be set, in each case, to unity (see, e.g., Guo and Tan 2011). Thus, we define the sum of the relative concentrations (or probabilities) of each component as 1, e.g., $Q_{\rm A} + Q_{\rm A}^- = 1$. The other intermediates, such as PQ, PC, Fd, ATP, and NADPH, are quantified in terms of pools (Ebenhöh et al. 2014), the sizes of which are expressed by using subscript "0," e.g., PQ₀, PC₀, Fd₀, ATP₀, and NADPH₀. These pools are constant for a given sample but vary from sample to sample. They are determined from experimental data in the model fitting process. Total concentrations of these intermediates are listed in Table 1.

The reactions shown in Eqs. 1–23 involve 20 state variables and are represented as x_i , i=1...20. Since the concentration of protons in the stoma is stable (Ebenhöh et al.

Table 2 State variables and their initial values; for abbreviations, see list of abbreviations

State variables	Symbol	Initial value
A*	x_1	0
P680*	x_2	0
P680 ⁺	x_3	0
Pheo-	x_4	0
$Q_{ m A}^-$	x_5	0
$Q_{ m B}^-$	x_6	0
$Q_{ m B}^{2-}$	x_7	0
PQ	x_8	PQ_0
PC ⁻	x_9	0
Fd ⁻	<i>x</i> ₁₀	0
N	<i>x</i> ₁₁	0
RuBP	<i>x</i> ₁₂	0
PGA	<i>x</i> ₁₃	PGA_0
DPGA	<i>x</i> ₁₄	0
PGAld	<i>x</i> ₁₅	0
ATP	<i>x</i> ₁₆	0
NADPH	<i>x</i> ₁₇	0
H_{lumen}^{+}	<i>x</i> ₁₈	0
$C_{\rm i}$	<i>x</i> ₁₉	C_a
Glucose	x_{20}	0

2011), it has not been treated as a variable in our model. The initial concentrations of some of the substances are considered as zero before photosynthetic activities start (i.e., after dark adaptation) or estimated from experimental data during the model fitting process. The state variables and initial conditions are listed in Table 2.



Based on the reactions described in the foregoing subsections, the 20 state variables are described by the following differential equations.

$$\frac{\mathrm{d}x_1}{\mathrm{d}t} = k_1 u (300 - x_1) - k_2 x_1 - k_3 (1 + x_{11}) x_1
- k_4 (1 - x_2 - x_3) x_1 + k_5 (300 - x_1) x_2$$
(24)

$$\frac{\mathrm{d}x_2}{\mathrm{d}t} = k_4 (1 - x_2 - x_3) x_1 - k_5 (300 - x_1) x_2 - k_6 x_2 (1 - x_4) + k_7 x_3 x_4 \tag{25}$$

$$\frac{\mathrm{d}x_3}{\mathrm{d}t} = k_6 x_2 (1 - x_4) - k_7 x_3 x_4 - 4k_8 x_3^4 \tag{26}$$

$$\frac{\mathrm{d}x_4}{\mathrm{d}t} = k_6 x_2 (1 - x_4) - k_7 x_3 x_4 - k_9 x_4 (1 - x_5) + k_{10} (1 - x_4) x_5 \tag{27}$$

$$\frac{\mathrm{d}x_5}{\mathrm{d}t} = k_9 x_4 (1 - x_5) - k_{10} (1 - x_4) x_5
- k_{11} x_5 (1 - x_6 - x_7) + k_{12} (1 - x_5) x_6
- k_{12} x_5 x_6 + k_{14} (1 - x_5) x_7$$
(28)

$$\frac{\mathrm{d}x_6}{\mathrm{d}t} = k_{11}x_5(1 - x_6 - x_7) - k_{12}(1 - x_5)x_6 - k_{13}x_5x_6 + k_{14}(1 - x_5)x_7 \tag{29}$$

$$\frac{\mathrm{d}x_7}{\mathrm{d}t} = k_{13}x_5x_6 - k_{14}(1 - x_5)x_7 - k_{15}x_7x_8 \tag{30}$$

$$\frac{\mathrm{d}x_8}{\mathrm{d}t} = -k_{15}x_7x_8 + k_{16}(PQ_0 - x_8)(PC_0 - x_9)^2 - k_{17}x_8x_9^2x_{18}^4 - k_{22}x_8x_{10}^2$$
(31)

$$\frac{\mathrm{d}x_9}{\mathrm{d}t} = 2k_{16} (PQ_0 - x_8)(PC_0 - x_9)^2 - 2k_{17}x_8x_9^2x_{18}^4
- k_{18}x_9 (Fd_0 - x_{10}) + k_{19} (PC_0 - x_9)x_{10}$$
(32)

$$\frac{\mathrm{d}x_{10}}{\mathrm{d}t} = k_{18}x_9 \left(\mathrm{Fd}_0 - x_{10} \right) - k_{19} \left(\mathrm{PC}_0 - x_9 \right) x_{10}
- 2k_{20}x_{10}^2 \left(\mathrm{NADPH}_0 - x_{17} \right)
+ 2k_{21} \left(\mathrm{Fd}_0 - x_{10} \right)^2 x_{17} - 2k_{22}x_{10}^2 x_8$$
(33)

$$\frac{\mathrm{d}x_{11}}{\mathrm{d}t} = k_{24}x_{18}(1 - x_{11}) - k_{25}x_{11} \tag{34}$$

$$\frac{\mathrm{d}x_{12}}{\mathrm{d}t} = -k_{26}x_{12}x_{19} + 3k_{29}x_{15}^5x_{16}^3 \tag{35}$$

$$\frac{\mathrm{d}x_{13}}{\mathrm{d}t} = 2k_{26}x_{12}x_{19} - k_{27}x_{13}x_{16} \tag{36}$$

$$\frac{\mathrm{d}x_{14}}{\mathrm{d}t} = k_{27}x_{13}x_{16} - k_{28}x_{14}x_{17} \tag{37}$$

$$\frac{\mathrm{d}x_{15}}{\mathrm{d}t} = k_{28}x_{14}x_{17} - 5k_{29}x_{15}^5x_{16}^3 - k_{31}x_{15} \tag{38}$$

$$\frac{\mathrm{d}x_{16}}{\mathrm{d}t} = 3k_{23}(ATP_0 - x_{16})^3 x_{18}^{14} - k_{27}x_{13}x_{16} - 3k_{29}x_{15}^5 x_{16}^3$$
 (39)

$$\frac{\mathrm{d}x_{17}}{\mathrm{d}t} = k_{20}x_{10}^2 \left(\text{NADPH}_0 - x_{17} \right) - k_{21}(\text{Fd}_0 - x_{10})^2 x_{17} - k_{28}x_{14}x_{17}$$
(40)

$$\frac{\mathrm{d}x_{18}}{\mathrm{d}t} = 4k_8 x_3^4 + 4k_{16} \left(PQ_0 - x_8 \right) \left(PC_0 - x_9 \right)^2 - 4k_{17} x_8 x_9^2 x_{18}^4
- 14k_{23} \left(ATP_0 - x_{16} \right)^3 x_{18}^{14}$$
(41)

$$\frac{\mathrm{d}x_{19}}{\mathrm{d}t} = k_{30} \left(C_{\mathrm{a}} - x_{19} \right) \tag{42}$$

$$\frac{\mathrm{d}x_{20}}{\mathrm{d}t} = \frac{1}{2}k_{31}x_{15} \tag{43}$$

Here, all the k_i constants (i=1...31) are reaction rate constants that are determined from experimental data as described below in "Model validation and simulation" section.

We note that chlorophyll *a* fluorescence (ChlF) has been widely used as a signature (measurable indicator) of photosynthesis (see, e.g. Govindjee 1995; Papageorgiou and Govindjee 2004; also see: Zhu et al. 2005) and is being used as the measurable output. ChlF emission rate is represented by the reaction in Eq. (2), and the measured ChlF intensity can be expressed as (see Guo and Tan 2011):

$$F = G * k_2 * x_1 \tag{44}$$

where G is an overall instrumentation gain constant, k_2 is the rate of dissipation by fluorescence, and x_1 is the concentration of A^* . PSI fluorescence is ignored here as stated above. State Eqs. (24–43) and the final Eq. (44) describe the major steps from light absorption to glucose synthesis.

Results and discussion

Model validation and simulation

To determine k_1 to k_{31} , G, and the pool sizes in the model, the Levenberg–Marquardt algorithm (Levenberg 1944; Marquardt 1963) was used to fit the model to the experimental data in order to check the applicability of our model. The experimental data that we used is reproduced from the Fig. 2



in Stirbet and Govindjee (2016). We used Matlab (Version 8.5, The Mathworks, Natick, MA) to program the algorithm. A relatively long time (say, e.g., 15 s) of experiments is desirable to estimate the reaction rates especially for the dark reactions in real applications. The focus of this work is to put forward a framework for photosynthetic activities and plant growth control strategy; the experiment and the data in this work only serve as a demonstration of the proposed concept and algorithm. After parameter estimation, the model, described above, was used to simulate the ChIF

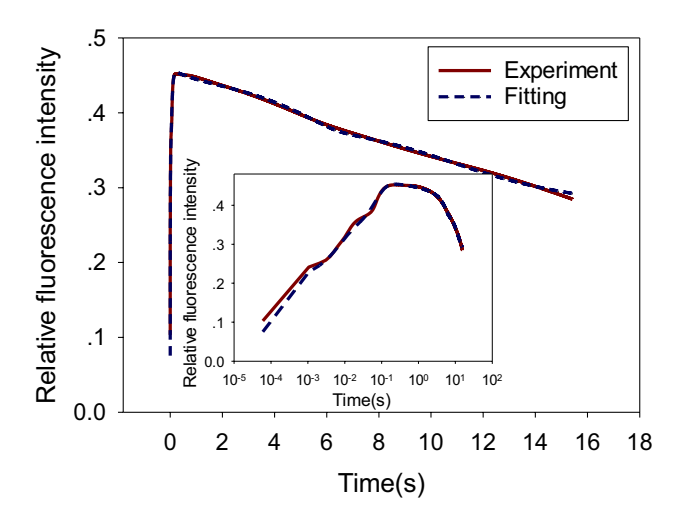


Fig. 2 Comparison of experimental and simulation results of time dependence of chlorophyll a fluorescence induction. The plot is presented on a linear time coordinate (main figure) and on a logarithmic time coordinate (the insert). The experimental data used are from Fig. 2 in Stirbet and Govindjee (2016), from leaves of *Pisum sativum* under 3000 μ mol photons m⁻² s⁻¹

Table 3 Estimated model parameters used for model prediction in Fig. 2

curve. Figure 2 shows that the model, developed in this study, fits quite well with the experimental values of chlorophyll fluorescence, and the estimated model parameters used are listed in Table 3. As discussed above, the reaction rates in the "second-order reaction kinetics" are effective rates but they still correspond to some known reactions. In addition, polypeptide composition of thylakoid membranes highly depends on the environmental conditions even for the same species. Under high temperature or heavy metal stress, the fluorescence curve will show differences, thus the different rates or pool sizes will be obtained through the method applied above, which will compensate for the changes in polypeptide of thylakoid membranes.

Relative errors were computed as:
$$\sqrt{\sum_{i=1}^{N}(y_i^*-y_i)^2} / \sqrt{\sum_{i=1}^{N}(y_i^*)^2}, \text{ where } y_i^* \text{ is the } i \text{th experimen-}$$

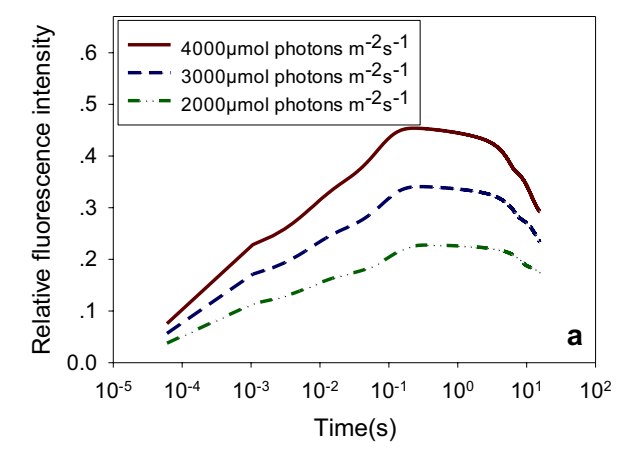
tally measured ChIF value and y_i is the *i*th model prediction, and N is the number of total data points. The average relative error was 0.028%, indicating a good fit of the model to the experimental data.

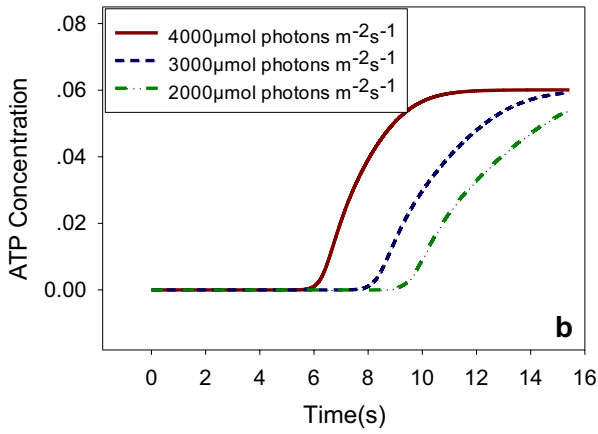
Figure 3 shows simulation results on chlorophyll a fluorescence transient (a PSII signal), ATP concentration (product of light reactions), and glucose concentration (product of dark reactions) during about 15 s, at three different light intensities. In these simulations, the concentration of external CO_2 is assumed to be the same in all cases. Figure 3a shows that as the light intensity increases, ChlF intensity increases due to higher light absorption that leads to higher PSII activity. Figure 3b shows the changes in [ATP] with time at three different light intensities. As the light intensity increases, the rate

Rate constant (see Eqs. 1–24)	Figure 2	Rate constant (see Eqs. 1–24)	Figure 2	Rate constant (see Eqs. 1–24)	Figure 2
k_1u	0.07	k ₁₄	26.24	k ₂₇	0.35
k_2	511.22	k ₁₅	13.02	k_{28}	0.0004
k_3	1507	k_{16}	31.76	k_{29}	1.878
k_4	2191	k_{17}	0.02	k ₃₀	5.96×10^{-5}
k_5	0.48	k_{18}	42.34	k ₃₁	4.7×10^{-5}
k_6	78.8	k_{19}	0.18	PQ_0	6.0
k_7	120.1	k_{20}	6.54	PC_0	1.5
k_8	3.19	k_{21}	17.58	Fd_0	46.7
k_9	65.5	k_{22}	95.35	ATP_0	0.06
k_{10}	65.0	k_{23}	35.87	$NADPH_0$	20.7
k_{11}	0.038	k_{24}	25.34	PGA_0	5.54
k_{12}	85.15	k ₂₅	63.74	G	0.08
k ₁₃	67.62	k_{26}	0.031		

For a given system, different model structures can be developed if the system is viewed from different angles; the system in this work was viewed as second-order reaction kinetics (for most reactions); further, it was highly simplified (see text). The reaction rates in this table cannot be compared with the reaction rates used for the first-order reaction kinetic model in the literature (see, e.g., Antal et al. 2013)







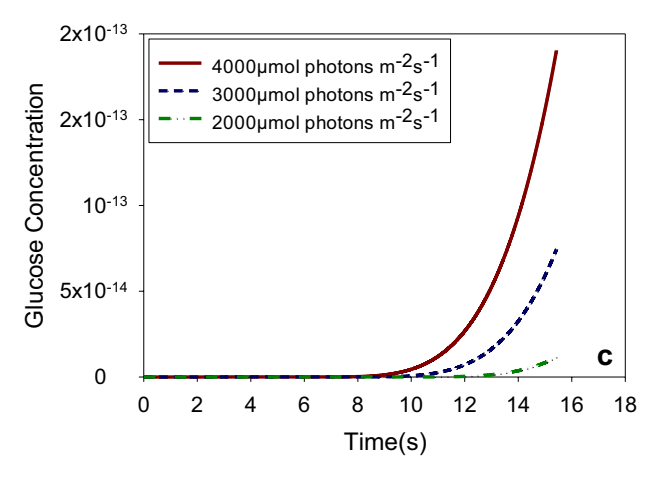
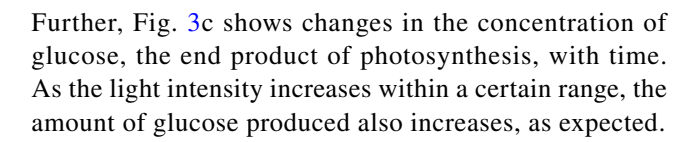


Fig. 3 Chlorophyll a fluorescence (a), ATP (b), and glucose (c) as a function of time, measured at three different light intensities

of electron transfer increases as well as hydrogen ions, deposited in the thylakoid lumen, resulting in a larger pH gradient and, thus, larger proton motive force difference between the inside and outside the thylakoid membrane. This, in turn, leads to increased [ATP]. However, since the total amount of ATP and ADP in the system is constant, ATP does not always increase when it reaches a certain level, which is shown by the model as seen in Fig. 3b.



Estimation of states and control of photosynthetic activities

With a process model, unmeasurable states may be estimated based on measured ChlF by using the extended Kalman filter (EKF) method (Chui and Chen 1998); consequently, a quantity related to photochemical reactions, though not directly measurable, may be controlled or influenced by changing light conditions or other variable conditions. Below, we illustrate this concept as well as the method.

Estimation of states based on chlorophyll fluorescence

Kalman (1960) had proposed a method based on a mathematical model for state estimation, in which values of state variables are estimated from the measured system output. This method has been widely used, such as in fault diagnosis, automation, radar systems, and missile tracking. The extended Kalman filter (EKF) developed later (Chui and Chen 1998) has mainly been used for state estimation of nonlinear systems and it is thus applicable to the photosynthesis model developed here. More information about the Kalman filter and the EKF can be found in Chui and Chen (1998).

The EKF algorithm was programmed in Matlab to estimate the values of state variables based on the process model developed in this study and the measured data on ChIF. Figure 4 shows a comparison between simulated glucose production as was shown in Fig. 3c (which is practically impossible to measure) and the values estimated by the EKF method from the measured ChIF. This comparison may not

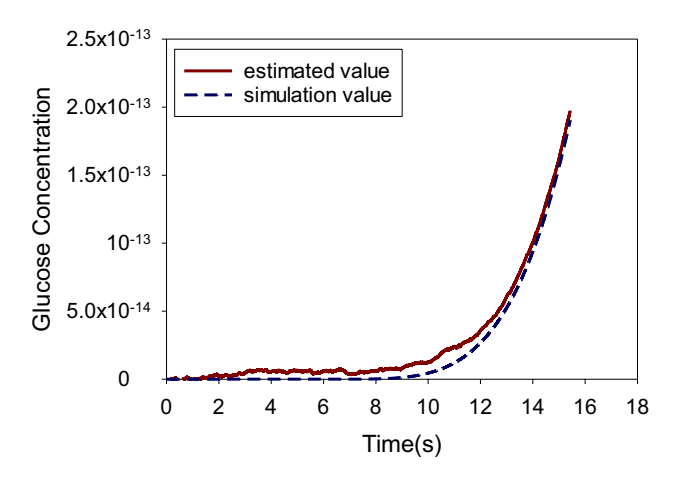


Fig. 4 Comparison of EKF-estimated glucose with simulated "true" values



appear very meaningful since both methods are based on the same model and the same measured data, and therefore, are expected to produce similar results; however, it shows that if we take the simulated glucose data to have the true value(s) from a sample process, these values can be successfully estimated from measured ChlF by using the EKF method and the process model.

Control of photosynthetic activities with a constant PQ reduction efficiency rate based on the extended Kalman filter method

The reaction quantity $v = k_{15}x_7x_8$, related to the reduction rate of PQ at a certain moment, is based on Eq. (10). In addition, the reduction rate of PQ reflects the transport speed of electrons in the PSII system, which is related to the overall photosynthetic efficiency. We believe that if we can artificially adjust the dynamic behavior of v, then we can further achieve the optimal control of plant growth in the future. The simplest and most commonly used PID (proportion, integral, and derivative) closed loop control system (see, e.g., Alvarez-Ramirez et al. 2003, for details of PID control) was adopted in this work to control the dynamics of v. It may reflect the number of electrons used for forward photochemical reactions, which should be positively related to the final biomass production. The values of x_7 and x_8 , which cannot

be practically measured, can be estimated by using the EKF method from the measured ChIF data.

Figure 5 shows a closed loop control system based on EKF. The controllable input is light intensity *u* and the measurable output is ChlF or *F*. In the diagram, the *controller* is a control algorithm such as PID. The power supply is an energy source for lighting such as light-emitting diodes (LED) or high-pressure sodium (HPS) lamps (Iersel et al. 2016). The *Light Regulator* regulates the lighting based on the controller output. The state observer is based on EKF and the process model developed here. The photosensor measures ChlF.

We used the PID control as shown in Fig. 5 to regulate the reduction speed (v) of PQ; v is usually not at a constant level when light intensity is constant because of the light protection mechanism and other reaction dynamics in the short period of time. However, for example, we may use the controller in Fig. 5 to regulate v around a constant setpoint V. Figure 6a shows the controlled lighting variations resulting from the PID controller to regulate PQ reduction speed at about a constant setpoint (Fig. 6b). Figure 6 shows that the PID controller drives PQ reduction speed to the setpoint quickly and then reduces illumination light to maintain v near a constant value. Constant levels of lighting intensities are often applied in greenhouse production, but a steady level of lighting may result in energy wastage and even

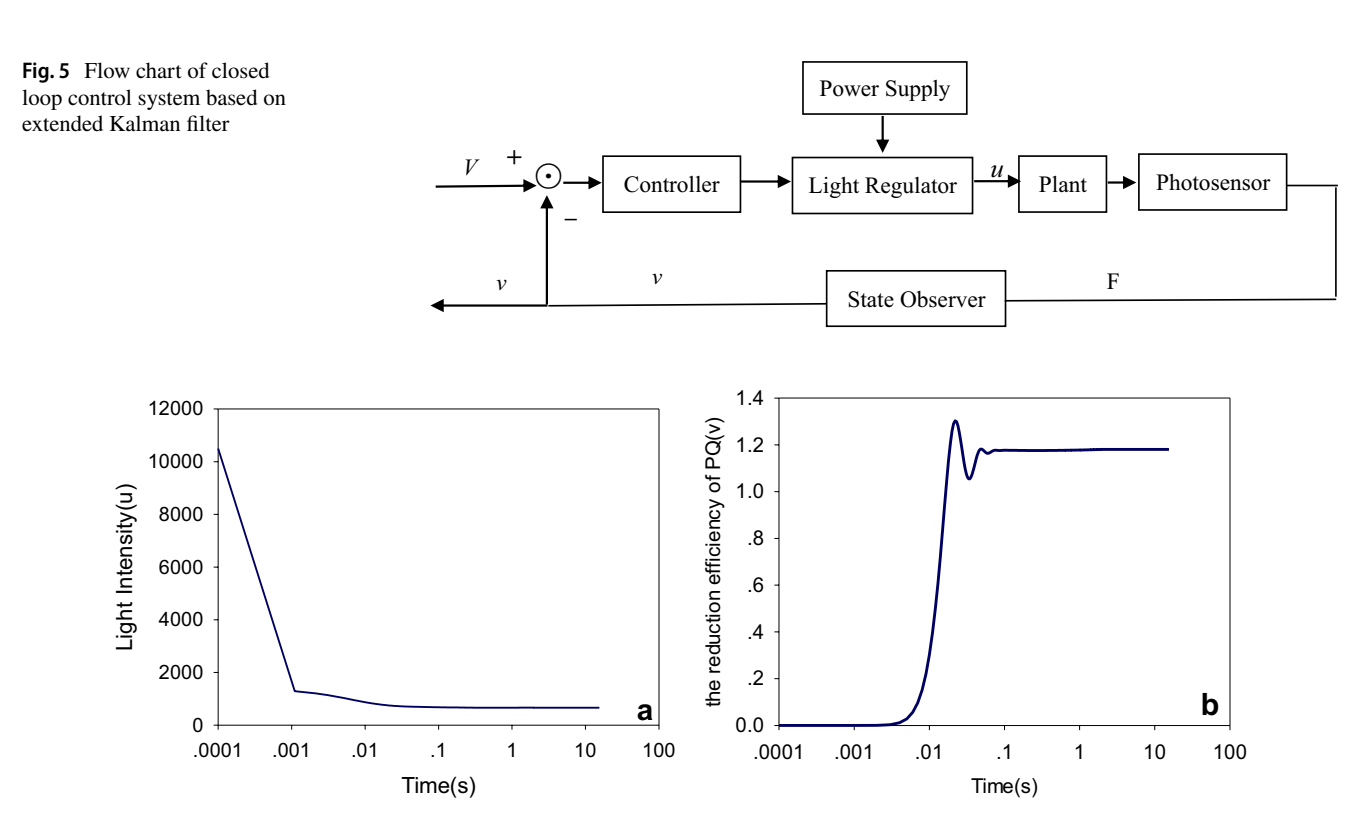


Fig. 6 PID (proportion, integral, and derivative) control of PQ reduction speed based on EKF state estimation and measured ChlF. a Control signal u (light intensity) in μ mol photons m⁻² s⁻¹ and **b** rate of reduction of PQ



reduce photosynthetic efficiency because of light protection mechanisms, or it may even damage the plants. This example demonstrates how the photosynthesis process may be altered to yield a desired dynamic behavior by using the model developed here along with the measured ChIF.

Conclusions

In this study, a minimized model structure was developed to describe the dynamically significant activities in the plant photosynthesis process. Some details such as those related to water oxidation (Kok-Joliot cycle) and photorespiration are not included in our current simplified analysis. After parameter optimization, the model, presented here, was, however, able to describe quite well experimentally measured chlorophyll fluorescence. The model was then used to show that unmeasurable state variables in the process may be estimated by using the extended Kalman filter (EKF) method. Finally, a feedback control framework has been proposed to alter or regulate photosynthetic activities by using an EKF-based state observer. The control framework is illustrated, in this study, with an example in which plastoquinone reduction is regulated with light intensity as a controllable input and chlorophyll fluorescence as a measured output. We emphasize that, on the one hand, we need to make the model as detailed as possible to describe the real system, but, on the other hand, we must make the model as simple as possible to develop a framework for controlling photosynthetic activities. We are aware that the model is not perfect and can be improved in the future, but it demonstrates the concept and potential of a plant growth control by using plant physiological signal as a feedback. This type of framework is important because it allows further development of optimal control for greenhouse production. This work serves as a launching point for further research on plant growth optimization and regulation.

Acknowledgements We thank Alexendrina (Sandra) Stirbet for her critical comments that led to improvement of our paper. This project was partially supported by National Natural Science Foundation of China (Nos: 51961125102, 31771680), Fundamental Research Funds for the Central Universities of China (No: JUSRP51730A), the Modern Agriculture Funds of Jiangsu Province (No: BE2018334), the 111 Project (B12018), and the Research Funds for New Faculty of Jiangnan University. Govindjee thanks the Department of Plant Biology and the Department of Biochemistry of the University of Illinois at Urbana-Champaign, for constant support.

Compliance with ethical standards

Conflict of interest The authors declare that they have no conflict of interest.

References

- Allen JF (2002) Photosynthesis of ATP—electrons, proton pumps, rotors, and poise. Cell 110:273–276
- Allen JF (2003) Cycle, pseudocyclic and noncyclic photophosphorylation: new links in the chain. Trend Plant Sci 8(1):1–19
- Alvarez-Ramirez J, Kelly R, Cervantes I (2003) Semiglobal stability of saturated linear pid control for robot manipulators. Automatica 39(6):989–995
- Antal TK, Kovalenko IB, Rubin AB, Tyystjärvi E (2013) Photosynthesis-related quantities for education and modeling. Photosynth Res 117:1–30
- Bassham JA (2003) Mapping the carbon reduction cycle: a personal retrospective. Photosynth Res 76:35–52
- Blankenship RE (2002) Origin and early evolution of photosynthesis. Blackwell Sci 256(2):42–48
- Buchanan B (2016) The carbon (formerly dark) reactions of photosynthesis. Photosynth Res 128(2):215–217
- Butler WL (1978) Energy distribution in the photochemical apparatus of photosynthesis. Annu Rev Plant Physiol 29:345–378
- Chui C, Chen G (1998) Kalman filtering with real-time applications, 3rd edn. Springer, Berlin, pp 19–45, 115–145
- Cramer WA, Kallas T (2015) Cytochrome complexes: evolution, structures, energy transduction, and signaling. Adv Photosynth Res 41:253–264
- Crofts AR (2004) The Q-cycle-a personal perspective. Photosynth Res 80(1–3):223–243
- Demmig-Adams B, Garab G, Adams W, Govindjee (2014) Non-photochemical quenching and energy dissipation in plants, algae and cyanobacteria. Adv Photosynth Res 40:45–72
- Ebenhöh O, Houwaart T, Lokstein H, Schlede S, Tirok K (2011) A minimal mathematical model of non-photochemical quenching of chlorophyll fluorescence. BioSystems 103:196–204
- Ebenhöh O, Fucile G, Finazzi G, Rochaix JD, Goldschmidt-Clermont M (2014) Short-term acclimation of the photosynthetic electron transfer chain to changing light: a mathematical model. Philos Trans R Soc Lond 369(1640):20130223
- Farquhar GD, Caemmerer SV, Berry JA (1980) A biochemical model of photosynthetic CO₂ assimilation in leaves of C3 species. Planta 149:78–90
- Feng S, Fu L, Xia Q, Tan J, Jiang Y, Guo Y (2018) Modeling and simulation of Photosystem II chlorophyll fluorescence transition from dark-adapted state to light-adapted State. IET Syst Biol 12(6):289–293
- Finazzi G, Johnson GN (2016) Cyclic electron flow: facts and hypotheses. Photosynth Res 129:227–230
- Golbeck JH (2006) Photosystem I: the light-driven plastocyanin: ferredoxin oxidoreductase. Adv Photsynth Res 24:155–175
- Gopal M (1996) Modern control system theory, 2nd edn. New Age International Limited, New Delhi
- Govindjee (1995) Sixty-three years since kautsky: chlorophyll a fluorescence. Aust J Plant Physiol 22:131–160
- Govindjee, Shevela D, Björn LO (2017) Evolution of the Z-scheme of photosynthesis. Photosynth Res 133:5–15
- Guo Y, Tan J (2011) Modeling and simulation of the initial phases of chlorophyll fluorescence from Photosystem II. BioSystems 103:152–157
- Guo Y, Tan J (2014) Kinetic Monte Carlo simulation of the initial phases of chlorophyll fluorescence from Photosystem II. Bio-Systems 115:1–4
- Guo Y, Tan J (2015) Recent advance in the application of chlorophyll a fluorescence from Photosystem II. Photochem Photobiol 91:1–14



- Harley PC, Thomas RB, Reynolds JF, Strain BR (1992) Modelling photosynthesis of cotton grown in elevated CO₂. Plant Cell Environ 15:271–282
- Iersel MW, Weaver G, Martin MT (2016) A chlorophyll fluorescence-based biofeedback system to control photosynthetic lighting in controlled environment agriculture. Am Soc Hort Sci 141(2):169–176
- Joët T, Cournac L, Peltier G, Havaux M (2002) Cyclic electron flow around photosystem I in C₃ plants. In vivo control by the redox state of chloroplasts and involvement of the NADH-dehydrogenase complex. Plant Physiol 128(2):760–769
- Junge W (2004) Protons, proteins and ATP. Photosynth Res 80(1-3):197-221
- Kalman RE (1960) A new approach to linear filtering and prediction problems. J Basic Eng Trans 82(Series D):35–45
- Katul GG, Ellsworth DS, Lai CT (2000) Modelling assimilation and intercellular CO₂ from measured conductance: a synthesis of approaches. Plant Cell Environ 23:1313–1328
- Kennedy D, Norman C (2005) What don't we know? Science 30(5731):75
- Kok B, Forbush B, McGloin M (1970) Cooperation of charges in photosynt hetic $\rm O_2$ Evolution-I. A linear four step mechanism. Photochem Photobiol 11:457–475
- Kramer DM, Evans JR (2011) The importance of energy balance in improving photosynthetic productivity. Plant Physiol 155:70–78
- Laisk A, Eichelman H, Oja V (2006) C3 photosynthesis in silico. Photosynth Res 90:45–66
- Lazár D (2006) The polyphasic chlorophyll a fluorescence rise measured under high intensity of exciting light. Funct Plant Biol 33:9–30
- Lazár D, Pospíšil P (1999) Mathematical simulation of chlorophyll a, fluorescence rise measured with 3-(3',4'-dichlorophenyl)-1,1-dimethylurea-treated barley leaves at room and high temperatures. Eur Biophys J 28(6):468–477
- Levenberg K (1944) A method for the solution of certain problems in least squares. Q Appl Math 2:164–168
- Mamedov M, Govindjee, Nadtochenko V, Semenov A (2017) Primary electrontransfer processes in photosynthetic reaction centers from oxygenic organisms. Photosynth Res 125:51–63
- Mar T, Govindjee (1972) Kinetic models of oxygen evolution in photosynthesis. J Theor Biol 36:427–446
- Marquardt DW (1963) An algorithm for least-squares estimation of nonlinear parameters. SIAM J Appl Math 11:431–441
- Matuszyńska A, Heidari S, Jahns P, Ebenhoh O (2016) A mathematical model of non-photochemical quenching to study short-term light memory in plants. Biochim Biophys Acta 1857:1860–1869
- Mirkovic T, Ostrumov EE, Anna JM, van Grondelle R, Govindjee, Scholes GD (2016) Light absorption and energy transfer in the antenna complexes of photosynthetic organisms. Chem Rev 117(2):249–293
- Najafpour M, Moghaddam AN, Shen JR, Govindjee (2013) Water oxidation and water oxidizing complex in cyanobacteria. In: Srivastava A et al (eds) Stress biology of cyanobacteria. Taylor & Francis, UK, pp 41–60
- Papageorgiou GC, Govindjee (2004) Chlorophyll a fluoresence: a signature of photosynthesis. Adv Photosynth Respir 19:757–778
- Papageorgiou GC, Govindjee (2014) The Non-photochemical quenching of the electronically excited state of chlorophyll a in plants: definitions, timelines, viewpoints, open questions. In:

- Demmig-Adams B, Garab G, Adams W, Govindjee (eds) Nonphotochemical quenching and energy dissipation in plants, algae and cyanobacteria. Springer, Dordrecht, pp. 1–44
- Portis AR (2003) Rubisco activase–Rubisco's catalytic chaperone. Photosynth Res 75:11–27
- Rabinowitch E, Govindjee (1969) Photosynthesis. Wiley http://www.life.illinois.edu/govindjee/g/Books.html; and http://www.life.illinois.edu/govindjee/photosynBook.html
- Sacksteder C, Kanazawa A, Jacoby M, Kramer D (2000) The proton to electron stoichiometry of steady-state photosynthesis in living plants: a proton-pumping Q cycle is continuously engaged. Proc Natl Acad Sci USA 9(26):14283–14288
- Shevela D, Eaton-Rye J, Shen J, Govindjee (2012) Photosystem II and unique role of bicarbonate: a historical perspective. Biochim Biophys Acta 1817:1134–1151
- Shevela D, Björn LO, Govindjee (2013) Oxygenic Photosynthesis. In: Razeghifard R (ed) Natural and artificial photosynthesis: solar power as an energy source. Wiley, Hoboken, pp 13–63
- Shevela D, Bjorn L, Govindjee (2019) Photosynthesis: solar energy for life. World Scientific, Singapore
- Snellenburg J, Johnson M, Ruban A, van Grondelle R, van Stokkum I (2017) A four state parametric model for the kinetics of non-photochemical quenching in Photosystem II. Biochim Biophys Acta 1858:854–864
- Stirbet A, Govindjee (2016) The slow phase of chlorophyll a fluorescence induction in silico: origin of the S-M fluorescence rise. Photosynth Res 130:193–213
- Stirbet A, Lazar D, Kromdijk J, Govindjee (2018) Chlorophyll a fluorescence induction: can just a one-second measurement be used to quantify abiotic stress responses? Photosynthesica 56(1):86–104
- Velthuys BR, Amesz J (1974) Charge accumulation at the reducing side of system 2 of photosynthesis. Biochim Biophys Acta 333(1):85–94
- Wang S, Tang H, Xia Q, Jiang Y, Tan J, Guo Y (2018) Modeling and simulation of photosynthetic activities in C3 plant as affected by CO₂. IET Syst Biol. https://doi.org/10.1049/iet-syb.2018.5064
- Winkler HH, Neuhaus HE (1999) Non-mitochondrial ATP transport. Trends Biochem Sci 24(2):64–68
- Wu A, Hammer GL, Doherty A, Caemmerer SV, Farquhar GD (2019) Quantifying impacts of enhancing photosynthesis on crop yield. Nat Plants 5:380–388
- Wydrzynski T, Satoh K (2005) Photosystem II: the light-driven water: plastoquinone oxidoreductase. Adv Photsynth Res 22:331–335
- Xia Q, Tan J, Ji X, Jiang Y, Guo Y (2018) Modeling and simulation of chlorophyll fluorescence from Photosystem II as affected by temperature. IET Syst Biol 12(6):304–310
- Zhu XG, Govindjee Baker NR, de Sturler E, Ort DR, Long SP (2005) Chlorophyll a fluorescence induction kinetics in leaves predicted from a model describing each discrete step of excitation energy and electron transfer associated with Photosystem II. Planta 223:114–133
- Zhu XG, Wang Y, Ort DR, Long SP (2013) e-photosynthesis: a comprehensive dynamic mechanistic model of C3 photosynthesis: from light capture to sucrose synthesis. Plant Cell Environ 36:1711–1727

Publisher's Note Springer Nature remains neutral with regard to jurisdictional claims in published maps and institutional affiliations.

